SIAM J. SCI. COMPUT.
Vol. 42, No. 4, pp. A2158–A2181

A STAGGERED CELL-CENTERED DG METHOD FOR LINEAR ELASTICITY ON POLYGONAL MESHES*

LINA ZHAO† AND EUN-JAE PARK‡

Abstract. We develop a new numerical method, namely, a locking-free staggered cell-centered discontinuous Galerkin method for linear elasticity on fairly general meshes. The method is well suited for general meshes possibly including hanging nodes; in particular, it does not deteriorate when the mesh becomes highly distorted. There are three unknowns involved in our formulation: stress, displacement, and rotation. The continuities of the three unknowns are staggered on the interelement boundaries. In addition, the symmetry of the stress tensor is imposed weakly by the introduction of Lagrange multipliers. Optimal a priori error estimates covering low regularities in L^2 errors of stress, displacement, and rotation are given; in addition, the locking-free error estimates are also investigated. Numerical experiments confirm the theoretical findings and verify the flexibility to rough grids and the locking-free property of the proposed method.

Key words. finite volume method, staggered grid, discontinuous Galerkin method, rough grid, locking-free, polygonal mesh

AMS subject classifications. 65N30, 65N50, 65N12

DOI. 10.1137/19M1278016

1. Introduction.

It is well known that the convergence rate for the standard displacement method using continuous linear finite elements deteriorates as the Lamé constant λ becomes large, i.e., when the elastic material is nearly incompressible (cf. [12]). This is a consequence of the fact that the convergence estimates are not uniform in λ, which, in turn, reflects the inability of the discretization space to accurately represent nontrivial solenoidal fields. Various methods have been proposed to circumvent this problem, for example, the p-version method [35], the PEERS method [5], the mixed method [34], and the nonconforming method [27]. All of the above-mentioned methods are defined on triangular meshes. In recent years, much effort has been devoted to the development and analysis of discretization methods that apply to more general meshes possibly featuring hanging nodes. In this context, we mention the hybrid high-order (HHO) method [24], virtual element method (VEM) [14, 8], weak Galerkin (WG) method [36], and staggered cell-centered finite element method (SC-FEM) [32].

The main difficulty arising in designing stable methods for linear elasticity is the symmetry constraint of the stress tensor. In principle, there are two approaches to designing stable methods for linear elasticity. The first approach is to enforce the symmetry of the stress tensor strongly; see [6, 1] and the references therein. One disadvantage of this approach is that sophisticated high-order polynomials for shape functions of the stress tensor are needed. The second approach is to impose the

*Submitted to the journal's Methods and Algorithms for Scientific Computing section July 29, 2019; accepted for publication (in revised form) April 21, 2020; published electronically July 14, 2020.

https://doi.org/10.1137/19M1278016

Funding: The work of the second author was supported by a National Research Foundation of Korea (NRF) grant funded by the Ministry of Science and ICT through grants NRF-2015R1A5A1009350 and NRF-2019R1A2C2090021.

†Department of Mathematics, The Chinese University of Hong Kong, Hong Kong SAR (lzhao@math.cuhk.edu.hk).

‡Department of Computational Science and Engineering, Yonsei University, Seoul 03722, Republic of Korea (ejpark@yonsei.ac.kr).

symmetry of stress weakly; we cite in particular the works [23, 5, 34, 15] in the direction of mixed finite element methods. In the context of mixed discontinuous Galerkin methods, few results are available [22, 33]. On the other hand, designing a numerical scheme that earns small degrees of freedom has been the subject of many papers [5, 3]. Therefore, the purpose of this paper is to develop a numerical scheme that is partially continuous and in mixed form involving a relatively small number of degrees of freedom. In addition, it is stable and accurate and is applicable to nearly incompressible problems.

Staggered discontinuous Galerkin (SDG) methods developed in [18, 19] have been successfully applied to a wide range of partial differential equations arising from practical applications. Adaptive mesh refinement based on guaranteed a posteriori error estimators has been well studied [20, 37]. SDG methods earn many distinctive features such as local and global conservations, stability and optimal convergence, and preservation of physical laws. In addition, the staggered continuity property of SDG methods naturally gives an interelement flux term without imposing additional numerical fluxes or penalty parameters, as is usually required by other DG methods. Recently, a staggered cell-centered DG (lowest order SDG) method for the Poisson equation on quadrilateral and polygonal meshes was initially proposed in [38] and extended to the Stokes equations [40] and the coupled Stokes–Darcy problem [39]. The purpose of this paper is to extend this approach to linear elasticity on polygonal meshes. The symmetry of stress is imposed weakly by the introduction of Lagrange multipliers (cf. [5]), which enters the system as a new variable that can be interpreted as the rotation of the displacement field. Namely, there are three unknowns involved in our formulation: stress, displacement, and rotation. As proposed in [38], we divide the initial polygonal mesh (primal mesh) into the union of triangles by connecting an interior point to the vertices. Then three finite element spaces composed of piecewise constant functions are defined on the resulting triangulations. The continuities of the three finite element spaces are staggered on the interelement boundaries. More precisely, there is one normal stress vector degree of freedom per dual edge, one displacement vector degree of freedom per dual mesh, and one rotation scalar degree of freedom per primal mesh. We note that our finite element function for rotation is different from the one proposed in [30], where the functions are discontinuous across the element boundaries, which leads to instability for the lowest order SDG method on general meshes.

Our method is indeed a finite volume method, where only a few works are based on rigorous mathematical analysis, for instance, [25, 29, 32]. In line with this development, we provide a rigorous analysis for the proposed method: A priori error analysis for stress, displacement, and rotation is given. Here we assume that the displacement $u \in H^{1+\epsilon}(\Omega;\mathbb{R}^2)$ and $0 < \epsilon \leq 1$. To the best of our knowledge, this is the first result on proving error estimates in L^2 errors of displacement, stress, and rotation for linear elasticity that allows low regularities, i.e., $0 < \epsilon < 1/2$. We also prove that the given error estimates do not suffer from the volumetric locking. We provide numerical evidence of the robustness of the proposed method; as expected, the method can be flexibly applied to rough grids and is locking free. We remark that the strategies of primal mesh and dual mesh exploited in this paper are quite similar to the SC-FEM proposed in [32], whereas our method employs piecewise constant functions for all the involved unknowns and the continuities of all the unknowns are staggered on the interelement boundaries.

In summary, our method has a number of advantages: First, our method only involves piecewise constant basis functions; thus, the computation can be carried out

simply without using any complicated quadrature rules. Second, the proposed method is suitable for fairly general meshes. In particular, it does not deteriorate when the mesh becomes highly distorted, which is highly appreciated from a practical point of view. Third, hanging nodes are allowed, which can be simply treated as additional vertices. Finally, a rigorous mathematical analysis covering the low regularity assumption is provided.

The rest of the paper is organized as follows. In the next section, the formulation of a lowest order SDG method for linear elasticity is given and stability is proved. In section 3, a priori error analysis for stress, displacement, and rotation are established. Then in section 4 the error estimates are proved to be robust in nearly incompressible problems. Some numerical experiments are carried out in section 5 to confirm the proposed theories, where the numerical results indicate that the proposed method allows rough grids and is locking free. Finally, in section 6 a conclusion is given.

2. The lowest order SDG method.

2.1. Preliminaries. For a bounded open subset $D \subset \mathbb{R}^2$, we use $L^2(D)$ to denote the Hilbert space of real-valued functions on D whose inner product and corresponding norm are

$$(p,q)_D := \int_D pq\, dx, \quad \|p\|_{0,D} := (p,p)_D^{\frac{1}{2}}, \quad p,q \in L^2(D).$$

When $D = \Omega$, we will use (p,q) and $\|p\|_0$ for simplicity. For $r > 0$, we adopt the standard notation for the Sobolev spaces $H^r(D)$ and their associated norms $\|\cdot\|_{r,D}$. We use the same symbol $(\cdot,\cdot)_D$ for scalar product in $L^2(D;\mathbb{R}^2)$ and $L^2(D;\mathbb{R}^{2\times 2})$. More precisely, $(u,v)_D = \sum_{i=1}^2 (u_i,v_i)_D$ for $u,v \in L^2(D;\mathbb{R}^2)$ and $(\boldsymbol{\sigma},\boldsymbol{\psi})_D = \sum_{i=1}^2\sum_{j=1}^2 (\sigma_{ij},\psi_{ij})_D$ for $\boldsymbol{\sigma},\boldsymbol{\psi} \in L^2(D;\mathbb{R}^{2\times 2})$. We denote by $\langle\cdot,\cdot\rangle_D$ the scalar product in $L^2(D)$, $D \subset \mathbb{R}$, and its vector and tensor versions. For $k \geq 0$, $P^k(D)$ is the space of polynomials on D of order $\leq k$, and the vector and tensor versions are defined by $P^k(D;\mathbb{R}^2)$ and $P^k(D;\mathbb{R}^{2\times 2})$, respectively. Throughout the paper, we use C to denote a generic positive constant, which may have a different value at different occurrences.

We define the differential operators for $v = (v_1,v_2)^T$ and $\boldsymbol{\psi} = (\psi_{ij})_{2\times 2}$:

$$\operatorname{grad} v = \begin{pmatrix} \frac{\partial v_1}{\partial x} & \frac{\partial v_1}{\partial y} \\ \frac{\partial v_2}{\partial x} & \frac{\partial v_2}{\partial y} \end{pmatrix}, \quad \varepsilon(v) = \begin{pmatrix} \frac{\partial v_1}{x} & \frac{1}{2}(\frac{\partial v_2}{\partial x} + \frac{\partial v_1}{\partial y}) \\ \frac{1}{2}(\frac{\partial v_2}{\partial x} + \frac{\partial v_1}{\partial y}) & \frac{\partial v_2}{\partial y} \end{pmatrix},$$

$$\operatorname{rot} v = -\frac{\partial v_1}{\partial y} + \frac{\partial v_2}{\partial x}, \quad \operatorname{div} \boldsymbol{\psi} = \left(\frac{\partial \psi_{11}}{\partial x} + \frac{\partial \psi_{12}}{\partial y}, \frac{\partial \psi_{21}}{\partial x} + \frac{\partial \psi_{22}}{\partial y}\right).$$

We also define two constant tensors,

$$\boldsymbol{\delta} = \begin{pmatrix} 1 & 0 \\ 0 & 1 \end{pmatrix}, \qquad \boldsymbol{\chi} = \begin{pmatrix} 0 & -1 \\ 1 & 0 \end{pmatrix},$$

and associate with any tensor $\boldsymbol{\psi}$ its trace and asymmetry,

$$\operatorname{tr}(\boldsymbol{\psi}) = \boldsymbol{\psi} : \boldsymbol{\delta}, \quad \operatorname{as}(\boldsymbol{\psi}) = \boldsymbol{\psi} : \boldsymbol{\chi},$$

where the colon indicates the scalar product of tensors given by

$$\boldsymbol{\psi} : \boldsymbol{\sigma} = \sum_{i=1}^2 \sum_{j=1}^2 \psi_{ij}\sigma_{ij}.$$

We now formulate the elasticity problem. For simplicity of exposition we restrict ourselves to a homogeneous isotropic body in a state of plane strain fixed at the boundary. The classical theory of linear elasticity then requires that

$$\boldsymbol{\sigma} = 2\mu\varepsilon(u) + \lambda \mathrm{tr}(\varepsilon(u))\boldsymbol{\delta} \quad \text{in } \Omega, \tag{2.1a}$$

$$-\mathrm{div}\,\boldsymbol{\sigma} = f \quad \text{in } \Omega, \tag{2.1b}$$

$$u = 0 \quad \text{on } \partial\Omega. \tag{2.1c}$$

Here u and $\boldsymbol{\sigma}$ denote the desired displacement and stress, f the imposed load, and μ and λ the positive Lamé constants. Inverting the stress-strain law (2.1a), setting $\gamma = (\mathrm{rot}\, u)/2$, and noting that

$$\varepsilon(u) = \mathrm{grad}\, u - \gamma\boldsymbol{\chi},$$

we see that

$$A\boldsymbol{\sigma} - \mathrm{grad}\, u + \gamma\boldsymbol{\chi} = 0 \quad \text{in } \Omega,$$

where $A\boldsymbol{\sigma} = \frac{1}{2\mu}\boldsymbol{\sigma} - \frac{\lambda}{4\mu(\mu+\lambda)}\mathrm{tr}(\boldsymbol{\sigma})\boldsymbol{\delta}$. We supplement this equation with the equilibrium condition (2.1a), the condition of symmetry of $\boldsymbol{\sigma}$ (implied by (2.1a)), and the fixed boundary condition (2.1c):

$$-\mathrm{div}\,\boldsymbol{\sigma} = f \quad \text{in } \Omega, \tag{2.2a}$$

$$\mathrm{as}(\boldsymbol{\sigma}) = 0 \quad \text{in } \Omega, \tag{2.2b}$$

$$u = 0 \quad \text{on } \partial\Omega. \tag{2.2c}$$

By imposing the symmetry of stress weakly as proposed in [5, 30], the weak formulation of (2.2) reads as follows: Find $(\boldsymbol{\sigma}, u, \gamma) \in L^2(\Omega;\mathbb{R}^{2\times 2}) \times H_0^1(\Omega;\mathbb{R}^2) \times L^2(\Omega)$ such that

$$a(\boldsymbol{\sigma},\boldsymbol{\psi}) - (\mathrm{grad}\, u, \boldsymbol{\psi}) + (\gamma, \mathrm{as}(\boldsymbol{\psi})) = 0 \qquad \forall \boldsymbol{\psi} \in L^2(\Omega;\mathbb{R}^{2\times 2}), \tag{2.3a}$$

$$(\boldsymbol{\sigma}, \mathrm{grad}\, v) = (f, v) \quad \forall v \in H_0^1(\Omega;\mathbb{R}^2), \tag{2.3b}$$

$$(\mathrm{as}(\boldsymbol{\sigma}), \eta) = 0 \qquad \forall \eta \in L^2(\Omega), \tag{2.3c}$$

where

$$a(\boldsymbol{\sigma},\boldsymbol{\psi}) = (A\boldsymbol{\sigma},\boldsymbol{\psi}).$$

2.2. Description of staggered cell-centered DG method. In this section, we describe the lowest order SDG method on general meshes and introduce some basic notation. In addition, the stability of the numerical scheme is also presented.

Three meshes will be constructed in our method: the primal meshes $\mathcal{T}_u$, the dual meshes $\mathcal{T}_d$, and the primal simplicial submeshes $\mathcal{T}_h$. For a polygonal domain Ω, consider a general mesh $\mathcal{T}_u$ (of Ω) that consists of nonempty connected close disjoint subsets of Ω:

$$\bar{\Omega} = \bigcup_{T\in\mathcal{T}_u} T.$$

We let $\mathcal{F}_u$ be the set of all primal edges in this partition and $\mathcal{F}_u^0$ be the subset of all interior edges, that is, the set of edges in $\mathcal{F}_u$ that do not lie on $\partial\Omega$. We construct

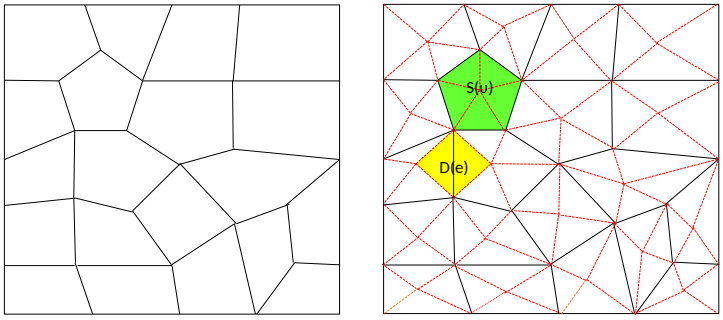

FIG. 1. *Schematic of the primal mesh $S(\nu)$, the dual mesh $D(e)$, and the primal simplexes.*

the primal submeshes $\mathcal{T}_h$ as a triangular subgrid of the primal grid: for an element $T \in \mathcal{T}_u$, elements of $\mathcal{T}_h$ are obtained by connecting the interior point ν to all vertices of $\mathcal{T}_u$ (see Figure 1):

$$\bar{\Omega} = \bigcup_{\tau \in \mathcal{T}_h} \bar{\tau}.$$

Here the interior point ν is selected as center point for simplicity, and we rename the union of the subtriangle sharing the common vertex ν by $S(\nu)$. Moreover, we will use $\mathcal{F}_p$ to denote the set of all the dual edges generated by this subdivision process. For each triangle $\tau \in \mathcal{T}_h$, we let h_τ be the diameter of τ and $h = \max\{h_\tau, \tau \in \mathcal{T}_h\}$. In addition, we define $\mathcal{F} := \mathcal{F}_u \cup \mathcal{F}_p$ and $\mathcal{F}^0 := \mathcal{F}_u^0 \cup \mathcal{F}_p$. The construction for polygonal meshes is illustrated in Figure 1, where the solid lines are edges in $\mathcal{F}_u$ and the dotted lines are edges in $\mathcal{F}_p$.

Finally, we construct the dual mesh. For each interior edge $e \in \mathcal{F}_u^0$, we use $D(e)$ to denote the dual mesh, which is the union of the two triangles in $\mathcal{T}_h$ sharing the edge e, and for each boundary edge $e \in \mathcal{F}_u \backslash \mathcal{F}_u^0$, we use $D(e)$ to denote the triangle in $\mathcal{T}_h$ having the edge e; see Figure 1. We write $\mathcal{T}_d$ as the union of all $D(e)$.

For each edge e, we define a unit normal vector n_e as follows: If $e \in \mathcal{F} \setminus \mathcal{F}^0$, then n_e is the unit normal vector of e pointing towards the outside of Ω. If $e \in \mathcal{F}^0$, an interior edge, we then fix n_e as one of the two possible unit normal vectors on e. When there is no ambiguity, we use n instead of n_e to simplify the notation.

We make the following mesh regularity assumptions throughout the paper (cf. [13, 17]).

Assumption 2.1. We assume the existence of constants $\rho_B, \rho_E > 0$ such that

(1) for every element $S(\nu) \in \mathcal{T}_u$ and every edge $e \subset \partial S(\nu)$, it satisfies $h_e \geq \rho_E h_{S(\nu)}$, where h_e denotes the length of edge e and $h_{S(\nu)}$ denotes the diameter of $S(\nu)$;

(2) every element $S(\nu)$ in $\mathcal{T}_u$ is star-shaped with respect to a ball of radius $\geq \rho_B h_{S(\nu)}$.

We remark that the above assumptions ensure that the triangulation $\mathcal{T}_h$ is shape regular.

For a scalar or vector function v belonging to broken Sobolev spaces, we define the jump as

$$[v] \mid_e = v \mid_{\tau_1} - v \mid_{\tau_2},$$

where τ_1 and τ_2 denote the two triangles which share the common edge $e \in \mathcal{F}^0$. For a subset $D \subset \mathbb{R}^2$, we define

$$H(\mathrm{div}, D) := \{q \in L^2(D;\mathbb{R}^2) : \mathrm{div}\, q \in L^2(D)\}.$$

In addition, we define the spaces

$$H(\mathrm{div}, D;\mathbb{R}^{2\times 2}) := \{\boldsymbol{\psi} \in L^2(D;\mathbb{R}^{2\times 2}) : \mathrm{div}\, \boldsymbol{\psi} \in L^2(D;\mathbb{R}^2)\}$$

and

$$H(\mathrm{div}, \mathcal{T}_u;\mathbb{R}^{2\times 2}) := \{\boldsymbol{\psi}\,|_{S(\nu)} \in H(\mathrm{div}, S(\nu);\mathbb{R}^{2\times 2})\ \forall S(\nu) \in \mathcal{T}_u\}.$$

Then the locally $H^1(\Omega)$–conforming SDG space S_h for the approximation of u can be defined by

$$S_h := \{v \in L^2(\Omega;\mathbb{R}^2) : v\,|_{D(e)} \in P^0(D(e);\mathbb{R}^2)\ \forall e \in \mathcal{F}_u; v\,|_\tau = 0 \text{ if } \partial\tau \cap \partial\Omega = e, e \in \mathcal{F}_u \backslash \mathcal{F}_u^0\}.$$

The locally $H(\mathrm{div}, \Omega)$–conforming SDG space $\boldsymbol{V}_h$ for the approximation of $\boldsymbol{\sigma}$ is defined by

$$\boldsymbol{V}_h := \{\boldsymbol{\psi} \in L^2(\Omega;\mathbb{R}^{2\times 2}) : \boldsymbol{\psi}\,|_\tau \in P^0(\tau;\mathbb{R}^{2\times 2})\ \forall \tau \in \mathcal{T}_h, [\boldsymbol{\psi} n]\,|_e = 0\ \forall e \in \mathcal{F}_p\}.$$

Finally, the locally $H^1(\Omega)$–conforming finite element space for the approximation of γ is defined as

$$M_h := \{\eta \in L^2(\Omega) : \eta\,|_{S(\nu)} \in P^0(S(\nu))\ \forall S(\nu) \in \mathcal{T}_u\}.$$

We now define norms for $\boldsymbol{V}_h$ and $S_h \times M_h$ by

$$\|\boldsymbol{\psi}\|_{0,h}^2 = \|\boldsymbol{\psi}\|_0^2 + \sum_{e\in\mathcal{F}_p} h_e \|\boldsymbol{\psi} n\|_{0,e}^2,$$

$$\|(v,\eta)\|_h^2 = \|\eta\|_0^2 + \sum_{e\in\mathcal{F}_p} h_e^{-1} \|[v]\|_{0,e}^2.$$

An application of scaling arguments implies that there exists a positive constant $C > 0$ independent of h such that

$$C\|\boldsymbol{\psi}\|_{0,h} \le \|\boldsymbol{\psi}\|_0 \le \|\boldsymbol{\psi}\|_{0,h} \quad \forall \boldsymbol{\psi} \in \boldsymbol{V}_h. \tag{2.4}$$

Following [19, 38], we define the following bilinear forms:

$$b_h(\boldsymbol{\psi}, v) = -\sum_{e\in\mathcal{F}_p} \langle \boldsymbol{\psi} n, [v]\rangle_e,$$

$$b_h^*(v, \boldsymbol{\psi}) = \sum_{e\in\mathcal{F}_u^0} \langle v, [\boldsymbol{\psi} n]\rangle_e.$$

The following discrete adjoint property holds by employing integration by parts:

$$b_h(\boldsymbol{\psi}, v) = b_h^*(v, \boldsymbol{\psi}) \quad \forall (\boldsymbol{\psi}, v) \in \boldsymbol{V}_h \times S_h. \tag{2.5}$$

Then the staggered cell-centered DG method for (2.1) can be read as follows: Find $(\boldsymbol{\sigma}_h, u_h, \gamma_h) \in \boldsymbol{V}_h \times S_h \times M_h$ such that

$$a(\boldsymbol{\sigma}_h, \boldsymbol{\psi}) - b_h^*(u_h, \boldsymbol{\psi}) + (\gamma_h, \mathrm{as}(\boldsymbol{\psi})) = 0 \qquad \forall \boldsymbol{\psi} \in \boldsymbol{V}_h, \tag{2.6a}$$

$$b_h(\boldsymbol{\sigma}_h, v) = (f, v) \quad \forall v \in S_h, \tag{2.6b}$$

$$(\mathrm{as}(\boldsymbol{\sigma}_h), \eta) = 0 \qquad \forall \eta \in M_h. \tag{2.6c}$$

Remark 2.2 (local conservation of mass and momentum). Taking $v = 1$ in (2.6b) to be identically one in each $D(e)$, we have

$$\langle \boldsymbol{\sigma}_h n_D, 1\rangle_{\partial D(e)} = (f, 1)_{D(e)},$$

where n_D is the outward unit normal vector of $D(e)$. Then taking $\eta = 1$ in (2.6c) to be identically one in each primal element $S(\nu)$, we can obtain

$$(\mathrm{as}(\boldsymbol{\sigma}_h), 1)_{S(\nu)} = 0 \quad \forall S(\nu) \in \mathcal{T}_u.$$

The next lemma states the discrete inf-sup condition.

LEMMA 2.3. *There exists $C > 0$ independent of h such that, for any $(0,0) \neq (v,\eta) \in S_h \times M_h$, one can find $0 \neq \boldsymbol{\psi} \in \boldsymbol{V}_h$ satisfying*

$$\frac{b(\boldsymbol{\psi}; v, \eta)}{\|(v,\eta)\|_h \|\boldsymbol{\psi}\|_{0,h}} \geq C,$$

where $b(\boldsymbol{\psi}; v, \eta) = -b_h(\boldsymbol{\psi}, v) + (\mathrm{as}(\boldsymbol{\psi}), \eta)$.

Proof. Let $S(\nu)$ denote the primal mesh belonging to $\mathcal{T}_u$, and define

$$\mathcal{F}_p^{S(\nu)} := \{e \in \mathcal{F}_p : e \subset S(\nu)\}.$$

Given $v \in S_h$, we define $\boldsymbol{\psi}_1 \in \boldsymbol{V}_h$ by

$$\boldsymbol{\psi}_1 n \mid_e = h_e^{-1}[v] \mid_e \quad \forall e \in \mathcal{F}_p^{S(\nu)},$$

which immediately gives

$$\|\boldsymbol{\psi}_1 n\|_{0,e}^2 \leq C h_e^{-2} \|[v]\|_{0,e}^2 \quad \forall e \in \mathcal{F}_p^{S(\nu)}.$$

An application of the scaling arguments implies

$$\|\boldsymbol{\psi}_1\|_{0,S(\nu)}^2 \leq C \sum_{e \in \mathcal{F}_p^{S(\nu)}} h_e \|\boldsymbol{\psi}_1 n\|_{0,e}^2.$$

Therefore, we can obtain

$$\|\boldsymbol{\psi}_1\|_{0,S(\nu)}^2 \leq C \sum_{e \in \mathcal{F}_p^{S(\nu)}} h_e^{-1} \|[v]\|_{0,e}^2 \tag{2.7}$$

and

$$h_e \|\boldsymbol{\psi}_1 n\|_{0,e}^2 \leq C h_e^{-1} \|[v]\|_{0,e}^2 \quad \forall e \in \mathcal{F}_p^{S(\nu)}.$$

Let s denote the mean value of $\eta - \mathrm{as}(\boldsymbol{\psi}_1)$ on $S(\nu)$, so

$$\|s\|_{0,S(\nu)} \leq C\Big(\|\boldsymbol{\psi}_1\|_{0,S(\nu)} + \|\eta\|_{0,S(\nu)}\Big).$$

Now, set

$$\boldsymbol{\psi}_2 = \boldsymbol{\psi}_1 + \frac{s}{2}\boldsymbol{\chi},$$

which yields the following estimate by using (2.7):

(2.8)
$$\|\boldsymbol{\psi}_2\|_{0,S(\nu)} \le C(\|\boldsymbol{\psi}_1\|_{0,S(\nu)} + \|s\|_{0,S(\nu)}) \le C\Big(\Big(\sum_{e\in\mathcal{F}_p^{S(\nu)}} h_e^{-1}\|[v]\|_{0,e}^2\Big)^{1/2} + \|\eta\|_{0,S(\nu)}\Big).$$

Moreover, we have

$$(\mathrm{as}(\boldsymbol{\psi}_2),\alpha)_{S(\nu)} = (\mathrm{as}(\boldsymbol{\psi}_1)+s,\alpha)_{S(\nu)} = (\eta,\alpha)_{S(\nu)} \quad \forall \alpha \in P^0(S(\nu)).$$

Let $n=(n^1,n^2)^T$, and $\boldsymbol{\psi}=\boldsymbol{\psi}_2-\boldsymbol{r}$, where

$$\boldsymbol{r} = \begin{pmatrix} -\frac{sn^2}{2n^1} & 0 \\ 0 & \frac{sn^1}{2n^2} \end{pmatrix}.$$

It follows from the definitions of $\boldsymbol{\psi}_2$ and $\boldsymbol{\psi}$ that

$$\boldsymbol{\psi} n = \boldsymbol{\psi}_1 n, \quad \mathrm{as}(\boldsymbol{\psi}) = \mathrm{as}(\boldsymbol{\psi}_2).$$

Then the triangle inequality and (2.8) imply

$$\|\boldsymbol{\psi}\|_{0,S(\nu)} \le C\Big(\|\boldsymbol{\psi}_1\|_{0,S(\nu)} + \|s\|_{0,S(\nu)}\Big) \le C\Big(\Big(\sum_{e\in\mathcal{F}_p^{S(\nu)}} h_e^{-1}\|[v]\|_{0,e}^2\Big)^{1/2} + \|\eta\|_{0,S(\nu)}\Big).$$

Finally, summing over all $S(\nu)\in\mathcal{T}_u$ and employing the preceding arguments yield

$$\begin{aligned} b(\boldsymbol{\psi};v,\eta) &= \sum_{e\in\mathcal{F}_p} \langle \boldsymbol{\psi} n,[v]\rangle_e + (\mathrm{as}(\boldsymbol{\psi}),\eta) \\ &= \sum_{S(\nu)\in\mathcal{T}_u} \Big(\sum_{e\in\mathcal{F}_p^{S(\nu)}} \langle \boldsymbol{\psi}_1 n,[v]\rangle_e + (\mathrm{as}(\boldsymbol{\psi}_2),\eta)_{S(\nu)}\Big) \\ &= \sum_{e\in\mathcal{F}_p} h_e^{-1}\|[v]\|_{0,e}^2 + \|\eta\|_0^2 \ge C\|\boldsymbol{\psi}\|_{0,h}\|(v,\eta)\|_h. \end{aligned}$$ ∎

By combining the coercivity of a and the discrete inf-sup condition given in Lemma 2.3, we have the following theorem, which can be proved analogously to Theorem 1 of [30]. Thus, we omit the proof for simplicity.

THEOREM 2.4. *Problem* (2.6) *is well-posed.*

Remark 2.5 (comparison to existing methods). Our proposed method is based on the mixed formulation and consists only of piecewise constant functions; thereby computation is particularly simple without using a quadrature rule or affine mapping. The stress tensor can be computed simultaneously without resorting to reconstruction or postprocessing. Thanks to the enforced staggered continuity property, no stabilization is required. In addition, our method has very low degrees of freedom, as indicated in Figure 2, whereas the hybrid high-order (HHO) method introduced in [24] is based on the primal formulation, and the lowest order HHO method for elasticity consists of piecewise linear polynomial space for displacement (see Figure 3); in addition, a local displacement reconstruction is needed in order to define the bilinear form.

Next, we compare our method with the PEERS element and Arnold–Falk–Winther (AFW) element, as shown in Table 1, where $S(\tau)$, $\boldsymbol{V}(\tau)$, and $M(\tau)$ denote the local

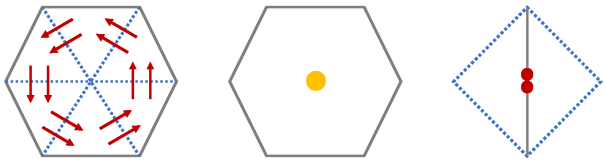

FIG. 2. *Degrees of freedom for stress (left), rotation (middle), and displacement (right) of our method.*

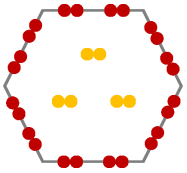

FIG. 3. *Face (red) and cell (orange) degrees of freedom for HHO method for* $k = 1$. *(Color available online.)*

TABLE 1
Comparison of staggered cell-centered DG, PEERS, and AFW.

Method	$S(\tau)$	$\boldsymbol{V}(\tau)$	$M(\tau)$	Element	Hanging nodes
staggered cell-centered DG	$P^0(\tau;\mathbb{R}^2)$	$P^0(\tau;\mathbb{R}^2)$	$P^0(\tau)$	polygon	$\surd$
PEERS [5]	$P^0(\tau;\mathbb{R}^2)$	$V_{\text{peers}}(\tau)$	$P^1(\tau)$	simplex	$\times$
AFW [7]	$P^0(\tau;\mathbb{R}^2)$	$P^1(\tau;\mathbb{R}^2)$	$P^0(\tau)$	simplex	$\times$

spaces defined on the triangle $\tau \in \mathcal{T}_h$ for the displacement, stress, and rotation, respectively; in addition, b_τ stands for the bubble function. For simplicity we use $\boldsymbol{V}(\tau)$ to indicate the first row of stress, and the Cartesian product of $V(\tau)$ generates the local space for stress. In addition, we define $V_{\text{peers}}(\tau) := P^0(\tau;\mathbb{R}^2) + P^0(\tau)\boldsymbol{x} + \text{rot}\, b_\tau$.

3. Error analysis. In this section, we will develop optimal a priori error estimates for stress, displacement, and rotation covering the low regularity assumption, i.e., $u \in H^{1+\epsilon}(\Omega;\mathbb{R}^2)$, $0 < \epsilon \le 1$.

3.1. Optimal convergence estimates. The primary goal of this subsection is to derive the error estimates for stress, displacement, and rotation. To begin with, we define the interpolation operators $I_h : H^1(\Omega;\mathbb{R}^2) \to S_h$ and $\pi_h : H^\epsilon(\Omega) \to M_h, 0 < \epsilon \le 1$ by

$$I_h v\,|_{D(e)} = \frac{1}{h_e}\int_e v\, ds \quad \forall e \in \mathcal{F}_u,$$
$$\pi_h q\,|_{S(\nu)} = \frac{1}{|S(\nu)|}\int_{S(\nu)} q\, dx \quad \forall S(\nu) \in \mathcal{T}_u,$$

where $|S(\nu)|$ denotes the area of $S(\nu)$.

The definition of I_h yields

$$b_h^*(v - I_h v, \boldsymbol{\psi}_h) = 0 \quad \forall \boldsymbol{\psi}_h \in \boldsymbol{V}_h. \tag{3.1}$$

We recall some interpolation estimates, which will be used for later analysis (cf. [21]):

$$\begin{aligned} &\|q - \pi_h q\|_0 \le Ch^\epsilon \|q\|_\epsilon \quad \forall q \in H^\epsilon(\Omega), 0 < \epsilon \le 1, \\ &\|v - I_h v\|_0 \le Ch\|v\|_1 \quad \forall v \in H^1(\Omega;\mathbb{R}^2). \end{aligned} \tag{3.2}$$

In addition, let $J_h\boldsymbol{\psi}$ be an interpolant of $\boldsymbol{\psi} \in H(\mathrm{div}, \mathcal{T}_u; \mathbb{R}^{2\times 2}) \cap H^{\epsilon}(\Omega; \mathbb{R}^{2\times 2})$ defined by

$$\langle (J_h\boldsymbol{\psi})n_e, \phi\rangle_e = \langle \boldsymbol{\psi} n_e, \phi\rangle_e \quad \forall \phi \in P^0(e; \mathbb{R}^2),\ e \in \mathcal{F}_p,$$

where we remark that the right side should be viewed as the duality pairing between $H^{\epsilon-1/2}(e; \mathbb{R}^2)$ and $H^{1/2-\epsilon}(e; \mathbb{R}^2)$ when $0 < \epsilon < 1/2$, and it arises from the formula

$$\langle \boldsymbol{\psi} n, \phi\rangle_{\partial\tau} := (\boldsymbol{\psi}, \mathrm{grad}\, L_\tau(\phi))_\tau + (\mathrm{div}\, \boldsymbol{\psi}, L_\tau(\phi))_\tau \quad \forall \tau \in \mathcal{T}_h, \tag{3.3}$$

where $L_\tau(\phi) \in H^{1-\epsilon}(\tau; \mathbb{R}^2)$ denotes the lifting of ϕ. Note that (3.3) is somewhat part of the folklore, and one can refer to [26] for a rigorous construction which avoids the above duality pairing.

By the definition of the bilinear form b_h, we get

$$b_h(J_h\boldsymbol{\psi} - \boldsymbol{\psi}, v) = 0 \quad \forall v \in S_h. \tag{3.4}$$

The following lemma illustrates the boundedness of the operator J_h (cf. [38]) when the above duality pairing is invoked to define J_h; cf. [25] otherwise.

LEMMA 3.1. *Let $0 < \epsilon < 1/2$ and $\boldsymbol{\psi} \in H^{\epsilon}(\tau; \mathbb{R}^{2\times 2}) \cap H(\mathrm{div}, \tau; \mathbb{R}^{2\times 2})$ for $\tau \in \mathcal{T}_h$. Then for $e \subset \partial\tau$, $\boldsymbol{\psi} n\,|_e \in H^{\epsilon-1/2}(e; \mathbb{R}^2)$, satisfying*

$$\|\boldsymbol{\psi} n\|_{\epsilon-1/2,e} \le C(\|\boldsymbol{\psi}\|_{\epsilon,\tau} + h_\tau^{1-\epsilon}\|\mathrm{div}\, \boldsymbol{\psi}\|_{0,\tau}).$$

Moreover, if $\boldsymbol{\psi} \in H^{\epsilon}(\Omega; \mathbb{R}^{2\times 2}) \cap H(\mathrm{div}, \mathcal{T}_u; \mathbb{R}^{2\times 2})$, then we have

$$\|J_h\boldsymbol{\psi}\|_0 \le C\Big(\Big(\sum_{\tau\in\mathcal{T}_h} h_\tau^2 \|\mathrm{div}\, \boldsymbol{\psi}\|_{0,\tau}^2\Big)^{1/2} + h^{\epsilon}\|\boldsymbol{\psi}\|_{\epsilon}\Big).$$

By using the boundedness of the interpolation operator J_h and a quotient space scaling argument, one can prove the following lemma (cf. [31]).

LEMMA 3.2. *Let $\boldsymbol{\psi} \in H^{\epsilon}(\Omega; \mathbb{R}^{2\times 2}) \cap H(\mathrm{div}, \Omega; \mathbb{R}^{2\times 2})$ for $0 < \epsilon \le 1$. Then there exists a positive constant C such that*

$$\|\boldsymbol{\psi} - J_h\boldsymbol{\psi}\|_0 \le Ch^{\epsilon}(\|\boldsymbol{\psi}\|_{\epsilon} + \|\mathrm{div}\, \boldsymbol{\psi}\|_0).$$

Now, we can state the next lemma, which yields the error estimate for L^2 errors of $\boldsymbol{\sigma}$ and γ.

THEOREM 3.3. *Let $(\boldsymbol{\sigma}, u, \gamma) \in H^{\epsilon}(\Omega; \mathbb{R}^{2\times 2}) \times H^{1+\epsilon}(\Omega; \mathbb{R}^2) \times H^{\epsilon}(\Omega), 0 < \epsilon \le 1$, and let $(\boldsymbol{\sigma}_h, u_h, \gamma_h)$ be the discrete solution of (2.6). Then there exists a positive constant C such that*

$$\|\boldsymbol{\sigma} - \boldsymbol{\sigma}_h\|_0 + \|\gamma - \gamma_h\|_0 \le Ch^{\epsilon}(\|\boldsymbol{\sigma}\|_{\epsilon} + \|\gamma\|_{\epsilon} + \|\mathrm{div}\, \boldsymbol{\sigma}\|_0).$$

Proof. First, it is easy to check that $(\boldsymbol{\sigma}, u, \gamma)$ satisfies the equations

$$a(\boldsymbol{\sigma}, \boldsymbol{\psi}) - b_h^*(u, \boldsymbol{\psi}) + (\gamma, \mathrm{as}(\boldsymbol{\psi})) = 0 \qquad \forall \boldsymbol{\psi} \in \boldsymbol{V}_h, \tag{3.5a}$$

$$b_h(\boldsymbol{\sigma}, v) = (f, v) \quad \forall v \in S_h, \tag{3.5b}$$

$$(\mathrm{as}(\boldsymbol{\sigma}), \eta) = 0 \qquad \forall \eta \in M_h. \tag{3.5c}$$

Then we have the following error equations by (2.6) and (3.5):

$$a(\boldsymbol{\sigma}-\boldsymbol{\sigma}_h,\boldsymbol{\psi})-b_h^*(u-u_h,\boldsymbol{\psi})+(\gamma-\gamma_h,\mathrm{as}(\boldsymbol{\psi}))=0 \quad \forall \boldsymbol{\psi}\in \boldsymbol{V}_h, \tag{3.6a}$$

$$b_h(\boldsymbol{\sigma}-\boldsymbol{\sigma}_h,v)=0 \quad \forall v\in S_h, \tag{3.6b}$$

$$(\mathrm{as}(\boldsymbol{\sigma}-\boldsymbol{\sigma}_h),\eta)=0 \quad \forall \eta\in M_h, \tag{3.6c}$$

which can be rewritten as

$$\begin{aligned} &a(J_h\boldsymbol{\sigma}-\boldsymbol{\sigma}_h,\boldsymbol{\psi})-b_h^*(I_hu-u_h,\boldsymbol{\psi})+(\pi_h\gamma-\gamma_h,\mathrm{as}(\boldsymbol{\psi}))\\ &\quad=a(J_h\boldsymbol{\sigma}-\boldsymbol{\sigma},\boldsymbol{\psi})-b_h^*(I_hu-u,\boldsymbol{\psi})+(\pi_h\gamma-\gamma,\mathrm{as}(\boldsymbol{\psi})) \quad \forall \boldsymbol{\psi}\in \boldsymbol{V}_h. \end{aligned} \tag{3.7}$$

We apply the discrete adjoint property (2.5) and Lemma 2.3 to get

$$\|\pi_h\gamma-\gamma_h\|_0 \le C \sup_{\boldsymbol{\psi}\in \boldsymbol{V}_h} \frac{-b_h^*(I_hu-u_h,\boldsymbol{\psi})+(\pi_h\gamma-\gamma_h,\mathrm{as}(\boldsymbol{\psi}))}{\|\boldsymbol{\psi}\|_0}, \tag{3.8}$$

which together with (3.1) and (3.7) yields

$$\|\pi_h\gamma-\gamma_h\|_0 \le C\Big(\|J_h\boldsymbol{\sigma}-\boldsymbol{\sigma}_h\|_0+\|J_h\boldsymbol{\sigma}-\boldsymbol{\sigma}\|_0+\|\pi_h\gamma-\gamma\|_0\Big). \tag{3.9}$$

Now, we will estimate $\|J_h\boldsymbol{\sigma}-\boldsymbol{\sigma}_h\|_0$. Equations (3.6a) and (3.6b) can be rewritten as follows by exploiting (3.1) and (3.4):

$$a(\boldsymbol{\sigma}-\boldsymbol{\sigma}_h,\boldsymbol{\psi})-b_h^*(I_hu-u_h,\boldsymbol{\psi})+(\gamma-\gamma_h,\mathrm{as}(\boldsymbol{\psi}))=0 \quad \forall \boldsymbol{\psi}\in \boldsymbol{V}_h, \tag{3.10}$$

$$b_h(J_h\boldsymbol{\sigma}-\boldsymbol{\sigma}_h,v)=0 \quad \forall v\in S_h. \tag{3.11}$$

Setting $\boldsymbol{\psi}=J_h\boldsymbol{\sigma}-\boldsymbol{\sigma}_h$ in (3.10), we obtain

$$a(\boldsymbol{\sigma}-\boldsymbol{\sigma}_h,J_h\boldsymbol{\sigma}-\boldsymbol{\sigma}_h)-b_h^*(I_hu-u_h,J_h\boldsymbol{\sigma}-\boldsymbol{\sigma}_h)+(\gamma-\gamma_h,\mathrm{as}(J_h\boldsymbol{\sigma}-\boldsymbol{\sigma}_h))=0.$$

We have from the discrete adjoint property (2.5), (3.4), (3.6b), and (3.6c)

$$b_h^*(I_hu-u_h,J_h\boldsymbol{\sigma}-\boldsymbol{\sigma}_h)=b_h(\boldsymbol{\sigma}-\boldsymbol{\sigma}_h,I_hu-u_h)=0, \quad (\pi_h\gamma-\gamma_h,\mathrm{as}(\boldsymbol{\sigma}_h-\boldsymbol{\sigma}))=0.$$

Therefore

$$\begin{aligned} a(J_h\boldsymbol{\sigma}-\boldsymbol{\sigma}_h,J_h\boldsymbol{\sigma}-\boldsymbol{\sigma}_h)&=-(\gamma-\pi_h\gamma,\mathrm{as}(J_h\boldsymbol{\sigma}-\boldsymbol{\sigma}_h))-(\pi_h\gamma-\gamma_h,\mathrm{as}(J_h\boldsymbol{\sigma}-\boldsymbol{\sigma}))\\ &\quad+a(J_h\boldsymbol{\sigma}-\boldsymbol{\sigma},J_h\boldsymbol{\sigma}-\boldsymbol{\sigma}_h). \end{aligned} \tag{3.12}$$

The coercivity of a, the Cauchy–Schwarz inequality, Young's inequality, and (3.12) yield

$$\|J_h\boldsymbol{\sigma}-\boldsymbol{\sigma}_h\|_0^2 \le C_{\varepsilon_1}(\|J_h\boldsymbol{\sigma}-\boldsymbol{\sigma}\|_0^2+\|\gamma-\pi_h\gamma\|_0^2)+\varepsilon_1(\|J_h\boldsymbol{\sigma}-\boldsymbol{\sigma}_h\|_0^2+\|\pi_h\gamma-\gamma_h\|_0^2).$$

Using (3.9) and taking ε_1 sufficiently small, one gets

$$\|J_h\boldsymbol{\sigma}-\boldsymbol{\sigma}_h\|_0 \le C'_{\varepsilon_1}(\|\boldsymbol{\sigma}-J_h\boldsymbol{\sigma}\|_0+\|\gamma-\pi_h\gamma\|_0).$$

Therefore

$$\|J_h\boldsymbol{\sigma}-\boldsymbol{\sigma}_h\|_0+\|\pi_h\gamma-\gamma_h\|_0 \le C(\|J_h\boldsymbol{\sigma}-\boldsymbol{\sigma}\|_0+\|\gamma-\pi_h\gamma\|_0).$$

Finally, we have from the triangle inequality, (3.2), and Lemma 3.2

$$\begin{aligned} \|\boldsymbol{\sigma}-\boldsymbol{\sigma}_h\|_0+\|\gamma-\gamma_h\|_0 &\le \|\boldsymbol{\sigma}-J_h\boldsymbol{\sigma}\|_0+\|J_h\boldsymbol{\sigma}-\boldsymbol{\sigma}_h\|_0+\|\gamma-\pi_h\gamma\|_0+\|\pi_h\gamma-\gamma_h\|_0\\ &\le Ch^{\epsilon}(\|\boldsymbol{\sigma}\|_{\epsilon}+\|\gamma\|_{\epsilon}+\|\mathrm{div}\,\boldsymbol{\sigma}\|_0). \end{aligned}$$

∎

Next, we prove the L^2 error estimate for displacement. For this purpose, we assume, for $g \in L^2(\Omega)$, the unique solution of

$$\operatorname{div} \tilde{\boldsymbol{\sigma}} = g \qquad \text{in } \Omega, \tag{3.13a}$$

$$A\tilde{\boldsymbol{\sigma}} + \operatorname{grad} \tilde{u} - \tilde{\gamma}\boldsymbol{\chi} = 0 \qquad \text{in } \Omega, \tag{3.13b}$$

$$as(\tilde{\boldsymbol{\sigma}}) = 0 \qquad \text{in } \Omega, \tag{3.13c}$$

$$\tilde{u} = 0 \qquad \text{on } \partial\Omega \tag{3.13d}$$

satisfies the following elliptic regularity estimate (cf. [28]):

$$\|\tilde{\boldsymbol{\sigma}}\|_\epsilon + \|\tilde{u}\|_{1+\epsilon} + \|\tilde{\gamma}\|_\epsilon \le C\|g\|_0. \tag{3.14}$$

THEOREM 3.4. *Let $(\boldsymbol{\sigma}, u, \gamma) \in H^\epsilon(\Omega; \mathbb{R}^{2\times 2}) \times H^{1+\epsilon}(\Omega; \mathbb{R}^2) \times H^\epsilon(\Omega), 0 < \epsilon \le 1$, and let $(\boldsymbol{\sigma}_h, u_h, \gamma_h)$ be the discrete solution of (2.6). Then there exists a positive constant C such that*

$$\|u - u_h\|_0 \le C\Big(h^{\min\{1,2\epsilon\}}(\|u\|_{1+\epsilon} + \|\gamma\|_\epsilon + \|\operatorname{div}\boldsymbol{\sigma}\|_0) + \Big(\sum_{\tau\in\mathcal{T}_h} h_\tau^2 \|f\|_{0,\tau}^2\Big)^{1/2}\Big).$$

Proof. Let $\tilde{\boldsymbol{\sigma}}, \tilde{u}$, and $\tilde{\gamma}$ be the solution of (3.13a)–(3.13c) with $g = I_h u - u_h$. Then we have from (3.14)

$$\|\tilde{\boldsymbol{\sigma}}\|_\epsilon + \|\tilde{u}\|_{1+\epsilon} + \|\tilde{\gamma}\|_\epsilon \le C\|I_h u - u_h\|_0. \tag{3.15}$$

Multiplying (3.13a) by $I_h u - u_h$, (3.13b) by $\boldsymbol{\sigma} - \boldsymbol{\sigma}_h$, and (3.13c) by $\gamma - \gamma_h$, and integrating over Ω yields

$$\begin{aligned}\|I_h u - u_h\|_0^2 = {}& (\operatorname{div}\tilde{\boldsymbol{\sigma}}, I_h u - u_h) + (A\tilde{\boldsymbol{\sigma}}, \boldsymbol{\sigma} - \boldsymbol{\sigma}_h) + (\operatorname{grad}(\tilde{u} - I_h\tilde{u}), \boldsymbol{\sigma} - \boldsymbol{\sigma}_h)\\ & - (\tilde{\gamma}, \operatorname{as}(\boldsymbol{\sigma} - \boldsymbol{\sigma}_h)) + (\operatorname{as}(\tilde{\boldsymbol{\sigma}}), \gamma - \gamma_h).\end{aligned}$$

We have from integration by parts, (3.1), and (3.6b)

$$\begin{aligned}\|I_h u - u_h\|_0^2 = {}& \sum_{e\in\mathcal{F}_p} \langle \tilde{\boldsymbol{\sigma}} n, [I_h u - u_h]\rangle_e + (A\tilde{\boldsymbol{\sigma}}, \boldsymbol{\sigma} - \boldsymbol{\sigma}_h) + \sum_{e\in\mathcal{F}_u^0} \langle \tilde{u} - I_h\tilde{u}, [(\boldsymbol{\sigma} - \boldsymbol{\sigma}_h)n]\rangle_e\\ & + \sum_{e\in\mathcal{F}_p} \langle [\tilde{u} - I_h\tilde{u}], (\boldsymbol{\sigma} - \boldsymbol{\sigma}_h)n\rangle_e - (\tilde{u} - I_h\tilde{u}, \operatorname{div}\boldsymbol{\sigma}) - (\tilde{\gamma}, \operatorname{as}(\boldsymbol{\sigma} - \boldsymbol{\sigma}_h))\\ & + (\operatorname{as}(\tilde{\boldsymbol{\sigma}}), \gamma - \gamma_h)\\ = {}& -b_h(\tilde{\boldsymbol{\sigma}}, I_h u - u_h) + a(\boldsymbol{\sigma} - \boldsymbol{\sigma}_h, \tilde{\boldsymbol{\sigma}}) + (f, \tilde{u} - I_h\tilde{u})\\ & - (\tilde{\gamma}, \operatorname{as}(\boldsymbol{\sigma} - \boldsymbol{\sigma}_h)) + (\operatorname{as}(\tilde{\boldsymbol{\sigma}}), \gamma - \gamma_h).\end{aligned}$$

The discrete adjoint property (2.5), (3.1), and (3.6a) imply

$$\begin{aligned}a(\boldsymbol{\sigma} - \boldsymbol{\sigma}_h, J_h\tilde{\boldsymbol{\sigma}}) &= b_h^*(u - u_h, J_h\tilde{\boldsymbol{\sigma}}) - (\gamma - \gamma_h, \operatorname{as}(J_h\tilde{\boldsymbol{\sigma}}))\\ &= b_h^*(I_h u - u_h, J_h\tilde{\boldsymbol{\sigma}}) - (\gamma - \gamma_h, \operatorname{as}(J_h\tilde{\boldsymbol{\sigma}}))\\ &= b_h(J_h\tilde{\boldsymbol{\sigma}}, I_h u - u_h) - (\gamma - \gamma_h, \operatorname{as}(J_h\tilde{\boldsymbol{\sigma}})).\end{aligned}$$

An application of the preceding arguments, (3.2), (3.4), and (3.6c) imply

$$\begin{aligned}\|I_h u - u_h\|_0^2 = {}& -b_h(\tilde{\boldsymbol{\sigma}} - J_h\tilde{\boldsymbol{\sigma}}, I_h u - u_h) + a(\boldsymbol{\sigma} - \boldsymbol{\sigma}_h, \tilde{\boldsymbol{\sigma}} - J_h\tilde{\boldsymbol{\sigma}}) + (f, \tilde{u} - I_h\tilde{u})\\ & - (\tilde{\gamma} - \pi_h\tilde{\gamma}, \operatorname{as}(\boldsymbol{\sigma} - \boldsymbol{\sigma}_h)) + (\gamma - \gamma_h, \operatorname{as}(\tilde{\boldsymbol{\sigma}} - J_h\tilde{\boldsymbol{\sigma}}))\\ = {}& a(\boldsymbol{\sigma} - \boldsymbol{\sigma}_h, \tilde{\boldsymbol{\sigma}} - J_h\tilde{\boldsymbol{\sigma}}) + (f, \tilde{u} - I_h\tilde{u}) - (\tilde{\gamma} - \pi_h\tilde{\gamma}, \operatorname{as}(\boldsymbol{\sigma} - \boldsymbol{\sigma}_h))\\ & + (\gamma - \gamma_h, \operatorname{as}(\tilde{\boldsymbol{\sigma}} - J_h\tilde{\boldsymbol{\sigma}})),\end{aligned}$$

which together with (3.2), Lemma 3.2, and the elliptic regularity estimate (3.15) implies

$$\|I_h u - u_h\|_0 \le C\Big(h^\epsilon(\|\boldsymbol{\sigma} - \boldsymbol{\sigma}_h\|_0 + \|\gamma - \gamma_h\|_0) + \Big(\sum_{\tau\in\mathcal{T}_h} h_\tau^2 \|f\|_{0,\tau}^2\Big)^{1/2}\Big). \tag{3.16}$$

Finally, we have from the triangle inequality, the optimal approximation properties (3.2), and Theorem 3.3

$$\begin{aligned}\|u - u_h\|_0 &\le \|u - I_h u\|_0 + \|I_h u - u_h\|_0 \\ &\le C\Big(h^{\min\{1,2\epsilon\}}(\|u\|_{1+\epsilon} + \|\gamma\|_\epsilon + \|\operatorname{div}\boldsymbol{\sigma}\|_0) + \Big(\sum_{\tau\in\mathcal{T}_h} h_\tau^2 \|f\|_{0,\tau}^2\Big)^{1/2}\Big). \quad \square\end{aligned}$$

Remark 3.5. By (3.16), we can obtain the following error estimate:

$$\|I_h u - u_h\|_0 \le C\Big(h^{2\epsilon}(\|\boldsymbol{\sigma}\|_\epsilon + \|\gamma\|_\epsilon + \|\operatorname{div}\boldsymbol{\sigma}\|_0) + \Big(\sum_{\tau\in\mathcal{T}_h} h_\tau^2 \|f\|_{0,\tau}^2\Big)^{1/2}\Big), \quad 0 < \epsilon \le 1. \tag{3.17}$$

When $0 < \epsilon \le 1/2$, we have $2\epsilon \le 1$; then we can get the optimal convergence rate up to order 2ϵ. However, for $1/2 < \epsilon \le 1$, we have $2\epsilon > 1$, which means the first part of the above term has better convergence (the term with respect to f only has first order convergence). The convergence rate can be improved to 2ϵ if f vanishes.

4. Locking-free error estimates. Locking refers to a phenomenon of numerical approximations for certain problems whose mathematical formulations involve a parameter dependency. For the linear elasticity problem, when the parameter $\lambda \to +\infty$ (i.e., when the material is nearly incompressible), it is well known that various finite element schemes, such as the continuous piecewise linear elements, result in poor observed convergence rates in the displacements; see [11] for a discussion of locking phenomena. We remark that the error analysis derived in Theorem 3.3 cannot guarantee that the involved constants are uniformly bounded as $\lambda \to +\infty$ because the coercivity constant of A on $L^2(\Omega;\mathbb{R}^{2\times 2})$ converges to 0 as $\lambda \to +\infty$ (cf. [30]).

In this section, we will show that the convergence rates for stress, displacement, and rotation are uniformly bounded for $\lambda \to +\infty$. For $\boldsymbol{\psi} \in L^2(\Omega;\mathbb{R}^{2\times 2})$ let $\boldsymbol{\psi}^D := \boldsymbol{\psi} - \frac{1}{2}\operatorname{tr}(\boldsymbol{\psi})\boldsymbol{\delta}$. We find the following lemma useful in the subsequent analysis (cf. Lemma 3.2 of [6]).

LEMMA 4.1. *For $\boldsymbol{\psi} \in L^2(\Omega;\mathbb{R}^{2\times 2})$, the inequality*

$$\|\boldsymbol{\psi}^D\|_0 \le C\|\boldsymbol{\psi}\|_A \tag{4.1}$$

holds with C depending only on μ.

LEMMA 4.2. *Let $(\boldsymbol{\sigma}, u, \gamma) \in H^\epsilon(\Omega;\mathbb{R}^{2\times 2}) \times H^{1+\epsilon}(\Omega;\mathbb{R}^2) \times H^\epsilon(\Omega)$, $0 < \epsilon \le 1$, and let $(\boldsymbol{\sigma}_h, u_h, \gamma_h)$ be the discrete solution of (2.6). Then the estimate*

$$\|(\boldsymbol{\sigma} - \boldsymbol{\sigma}_h)^D\|_0 + \|\gamma - \gamma_h\|_0 \le Ch^\epsilon(\|\boldsymbol{\sigma}\|_\epsilon + \|\gamma\|_\epsilon + \|\operatorname{div}\boldsymbol{\sigma}\|_0)$$

holds with C uniformly bounded as $\lambda \to +\infty$.

Proof. By the triangle inequality, Lemma 4.1, and the fact that $\|\boldsymbol{\psi}^D\|_0 \le C\|\boldsymbol{\psi}\|_0$, we can get

$$\begin{aligned}\|(\boldsymbol{\sigma}-\boldsymbol{\sigma}_h)^D\|_0 &\le \|(\boldsymbol{\sigma}-J_h\boldsymbol{\sigma})^D\|_0 + \|(J_h\boldsymbol{\sigma}-\boldsymbol{\sigma}_h)^D\|_0\\ &\le C(\|\boldsymbol{\sigma}-J_h\boldsymbol{\sigma}\|_0 + \|J_h\boldsymbol{\sigma}-\boldsymbol{\sigma}_h\|_A).\end{aligned}$$

Equations (3.7) and (3.8) and the fact $\|\cdot\|_A \le C\|\cdot\|_0$ with C independent of λ imply

$$\begin{aligned}\|\pi_h\gamma-\gamma_h\|_0 &\le C\sup_{\boldsymbol{\psi}\in\boldsymbol{V}_h}\frac{a(\boldsymbol{\sigma}_h-\boldsymbol{\sigma},\boldsymbol{\psi})+(\pi_h\gamma-\gamma,\mathrm{as}(\boldsymbol{\psi}))}{\|\boldsymbol{\psi}\|_0}\\ &\le C\Big(\|\boldsymbol{\sigma}-\boldsymbol{\sigma}_h\|_A+\|\gamma-\pi_h\gamma\|_0\Big)\\ &\le C\Big(\|\boldsymbol{\sigma}-J_h\boldsymbol{\sigma}\|_0+\|J_h\boldsymbol{\sigma}-\boldsymbol{\sigma}_h\|_A+\|\gamma-\pi_h\gamma\|_0\Big).\end{aligned}\tag{4.2}$$

Recall that (cf. (3.12))

$$a(J_h\boldsymbol{\sigma}-\boldsymbol{\sigma}_h, J_h\boldsymbol{\sigma}-\boldsymbol{\sigma}_h) = -(\gamma-\gamma_h,\mathrm{as}(J_h\boldsymbol{\sigma}-\boldsymbol{\sigma})) + a(J_h\boldsymbol{\sigma}-\boldsymbol{\sigma}, J_h\boldsymbol{\sigma}-\boldsymbol{\sigma}_h).\tag{4.3}$$

Notice that

$$(\mathrm{as}(A\boldsymbol{\psi}),\eta) = \frac{1}{2\mu}(\mathrm{as}(\boldsymbol{\psi}),\eta)\quad \forall\eta\in L^2(\Omega;\mathbb{K}),$$

where $\mathbb{K}$ denotes the set of all skew-symmetric 2×2 matrices.

Then (4.3) can be rewritten as

$$\begin{aligned}\|J_h\boldsymbol{\sigma}-\boldsymbol{\sigma}_h\|_A^2 = a(J_h\boldsymbol{\sigma}-\boldsymbol{\sigma}, J_h\boldsymbol{\sigma}-\boldsymbol{\sigma}_h) &- 2\mu(\gamma-\pi_h\gamma,\mathrm{as}(A(J_h\boldsymbol{\sigma}-\boldsymbol{\sigma})))\\ &- 2\mu(\pi_h\gamma-\gamma_h,\mathrm{as}(A(J_h\boldsymbol{\sigma}-\boldsymbol{\sigma}))).\end{aligned}$$

Young's inequality with the $\|\cdot\|_A$ norm gives

$$\|J_h\boldsymbol{\sigma}-\boldsymbol{\sigma}_h\|_A^2 \le C_{\varepsilon_1}(\|\boldsymbol{\sigma}-J_h\boldsymbol{\sigma}\|_A^2+\|\gamma-\pi_h\gamma\|_A^2)+\varepsilon_1(\|J_h\boldsymbol{\sigma}-\boldsymbol{\sigma}_h\|_A^2+\|\pi_h\gamma-\gamma_h\|_0^2),\tag{4.4}$$

which gives the desired estimate for $\|J_h\boldsymbol{\sigma}-\boldsymbol{\sigma}_h\|_A$ by taking ε_1 sufficiently small. The proof is complete by combining (3.2), Lemma 3.2, (4.2), and (4.4). ∎

THEOREM 4.3. *Let $(\boldsymbol{\sigma},u,\gamma)\in H^\epsilon(\Omega;\mathbb{R}^{2\times 2})\times H^{1+\epsilon}(\Omega;\mathbb{R}^2)\times H^\epsilon(\Omega)$, $0<\epsilon\le 1$, and let $(\boldsymbol{\sigma}_h,u_h,\gamma_h)$ be the discrete solution of* (2.6)*. Then the estimate*

$$\|\boldsymbol{\sigma}-\boldsymbol{\sigma}_h\|_0 \le C\Big(h^\epsilon(\|\boldsymbol{\sigma}\|_\epsilon+\|\gamma\|_\epsilon+\|\mathrm{div}\,\boldsymbol{\sigma}\|_0)+\Big(\sum_{\tau\in\mathcal{T}_h}h_\tau^2\|f\|_{0,\tau}^2\Big)^{1/2}\Big)$$

holds with C uniformly bounded as $\lambda\to+\infty$.

Proof. By the triangle inequality, $\|\boldsymbol{\sigma}-\boldsymbol{\sigma}_h\|_0 \le \|(\boldsymbol{\sigma}-\boldsymbol{\sigma}_h)^D\|_0 + \|\mathrm{tr}(\boldsymbol{\sigma}-\boldsymbol{\sigma}_h)\boldsymbol{\delta}\|_0$. If we take $\boldsymbol{\psi}=\boldsymbol{\delta}$ in (3.6a), then

$$(A(\boldsymbol{\sigma}-\boldsymbol{\sigma}_h),\boldsymbol{\delta}) = \frac{1}{2\mu+2\lambda}\int_\Omega \mathrm{tr}(\boldsymbol{\sigma}-\boldsymbol{\sigma}_h)\,dx = 0.$$

So $\mathrm{tr}(\boldsymbol{\sigma}-\boldsymbol{\sigma}_h)$ is mean value zero. It is known (cf. Lemma 5.4.2 of [10]) that there is $w\in H_0^1(\Omega;\mathbb{R}^2)$ such that

$$\mathrm{div}\,w = \mathrm{tr}(\boldsymbol{\sigma}-\boldsymbol{\sigma}_h),\quad \|w\|_1 \le C\|\mathrm{tr}(\boldsymbol{\sigma}-\boldsymbol{\sigma}_h)\|_0.\tag{4.5}$$

Then

$$\begin{aligned}\|\mathrm{tr}(\boldsymbol{\sigma}-\boldsymbol{\sigma}_h)\|_0^2 &= (\mathrm{tr}(\boldsymbol{\sigma}-\boldsymbol{\sigma}_h), \mathrm{div}\, w)\\ &= (\mathrm{tr}(\boldsymbol{\sigma}-\boldsymbol{\sigma}_h)\boldsymbol{\delta}, \mathrm{grad}\, w)\\ &= 2((\boldsymbol{\sigma}-\boldsymbol{\sigma}_h)-(\boldsymbol{\sigma}-\boldsymbol{\sigma}_h)^D, \mathrm{grad}\, w).\end{aligned}$$

By the Cauchy–Schwarz inequality and the inequality in (4.5), we have

$$((\boldsymbol{\sigma}-\boldsymbol{\sigma}_h)^D, \mathrm{grad}\, w) \le C\|(\boldsymbol{\sigma}-\boldsymbol{\sigma}_h)^D\|_0 \|\mathrm{tr}(\boldsymbol{\sigma}-\boldsymbol{\sigma}_h)\|_0.$$

It remains to estimate $(\boldsymbol{\sigma}-\boldsymbol{\sigma}_h, \nabla w)$. From integration by parts, (3.1), and (3.6b), we have

$$\begin{aligned}(\boldsymbol{\sigma}-\boldsymbol{\sigma}_h, \mathrm{grad}\, w) &= (\boldsymbol{\sigma}-\boldsymbol{\sigma}_h, \mathrm{grad}(w-I_h w))\\ &= \sum_{e\in\mathcal{F}_p} \langle(\boldsymbol{\sigma}-\boldsymbol{\sigma}_h)n, [w-I_h w]\rangle_e\\ &\quad + \sum_{e\in\mathcal{F}_u^0} \langle[(\boldsymbol{\sigma}-\boldsymbol{\sigma}_h)n], w-I_h w\rangle_e + (f, w-I_h w)\\ &= (f, w-I_h w).\end{aligned}$$

An application of the optimal approximation properties (3.2) implies

$$(\boldsymbol{\sigma}-\boldsymbol{\sigma}_h, \mathrm{grad}\, w) = (f, w-I_h w) \le C\Big(\sum_{\tau\in\mathcal{T}_h} h_\tau^2 \|f\|_{0,\tau}^2\Big)^{1/2} \|w\|_1.$$

Therefore

$$\|\mathrm{tr}(\boldsymbol{\sigma}-\boldsymbol{\sigma}_h)\|_0 \le C\Big(\|(\boldsymbol{\sigma}-\boldsymbol{\sigma}_h)^D\|_0 + \Big(\sum_{\tau\in\mathcal{T}_h} h_\tau^2 \|f\|_{0,\tau}^2\Big)^{1/2}\Big),$$

which, combined with Lemma 4.2, gives the desired estimate. ∎

Remark 4.4. By the estimate given in Lemma 4.2 and Theorem 4.3, it is easy to see that the estimate for $\|u-u_h\|_0$ also holds uniformly with $\lambda \to +\infty$ (cf. Theorem 3.4).

Remark 4.5 (extension to 3D). In this paper, we restrict our discussion to 2D for simplicity. In 3D, we first decompose the computational domain into the union of polyhedral meshes, then we connect an interior point to all the vertices of the polyhedral meshes. Thereby, the primal elements and dual elements are generated during this subdivision process. Then we can define our staggered spaces similarly to 2D; more precisely, the space for displacement is a constant vector over each dual element, the space for stress is a piecewise constant 2×2 tensor over the primal polyhedral meshes and is continuous in the normal direction over the dual faces, and the space for rotation is a constant function over each polyhedral meshes. We can count the degrees of freedom for our space in 3D: the number of degrees of freedom for displacement is $2N_{\mathrm{dual}}$, the number of degrees of freedom for stress is $2N_F$, and the number of degrees of freedom for rotation is N_{prm}, where N_{dual}, N_F, and N_{prm} represent the number of dual elements, the number of dual faces, and the number of primal elements, respectively. As for the analysis, we can again define projection operators I_h, J_h, and π_h similarly to 2D, which are polynomial preserving operators; then we can exploit the theory developed in [16] to derive the interpolation error estimates for the projection operators. The subsequent convergence analysis can be done in a similar way to 2D.

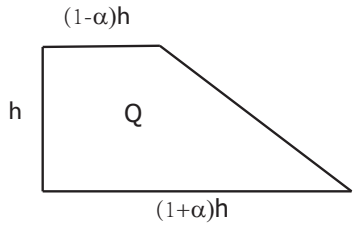

FIG. 4. *Schematic of trapezoidal grid.*

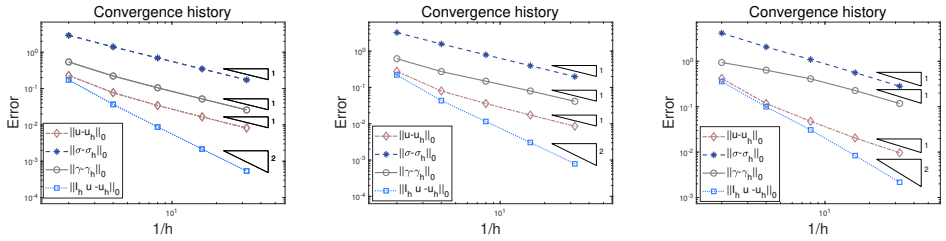

(a) (b) (c)

FIG. 5. *Convergence history on different types of grids for the example in section* 5.1. (a) *Unit square grid with* $\alpha = 0$. (b) *Trapezoidal grid with* $\alpha = 0.4$. (c) *Trapezoidal grid with* $\alpha = 0.8$.

5. Numerical experiments.

5.1. Smooth solution on unit square domain. In this example, we consider the unit square domain $(0,1)^2$ such that the exact solution is given by

$$u(x,y) = \begin{pmatrix} \sin(\pi x)\sin(\pi y) \\ x(1-x)y(1-y) \end{pmatrix}$$

and the right-hand side f can be calculated correspondingly.

We first partition the domain into uniform squares of size $h := 2^{-J}$, $J = 1, 2, \ldots$. Then we distort each element by pulling or pushing the vertices alternatively by a factor of α as proposed in [4] and shown in Figure 4. We choose the material parameters as $\lambda = 1$ and $\mu = 1$. The convergence history with respect to the mesh size with various values of α is displayed in Figure 5. Optimal convergence rates matching the proposed theories can be observed, and second order convergence can be achieved for $\|I_h u - u_h\|_0$. In addition, we note that with different values of α, the accuracy for $\boldsymbol{\sigma}$ and u is slightly changed, while the accuracy for γ seems to decrease as α increases. This is probably because γ is defined over the initial partition; the shape of the initial partition can influence the accuracy. Next, the convergence history on the Voronoi mesh is displayed in Figure 6, where first order convergence can be achieved for L^2 errors of $\boldsymbol{\sigma}, u, \gamma$, and, in addition, second order convergence can be obtained for $\|I_h u - u_h\|_0$.

5.2. Locking-free test. To check the locking-free property of the proposed numerical scheme, we consider the 2D domain $\Omega = (0,1)^2$ with the exact solution given by

$$u(x,y) = \begin{pmatrix} \sin(\pi x)\sin(\pi y) + \frac{1}{2\lambda}x \\ \cos(\pi x)\cos(\pi y) + \frac{1}{2\lambda}y \end{pmatrix} \tag{5.1}$$

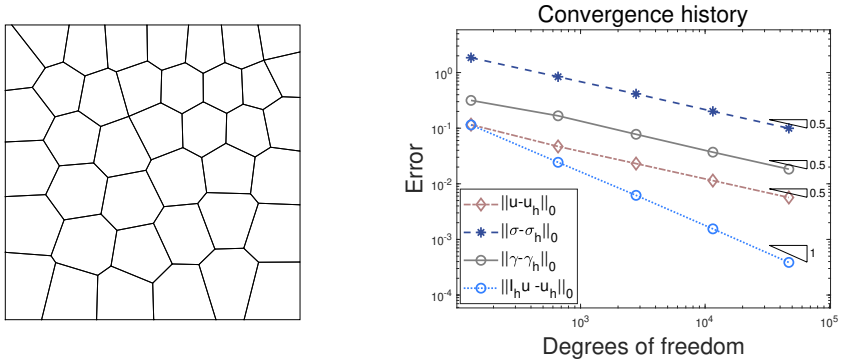

FIG. 6. *Voronoi mesh (left) and convergence history (right) for the example in section* 5.1.

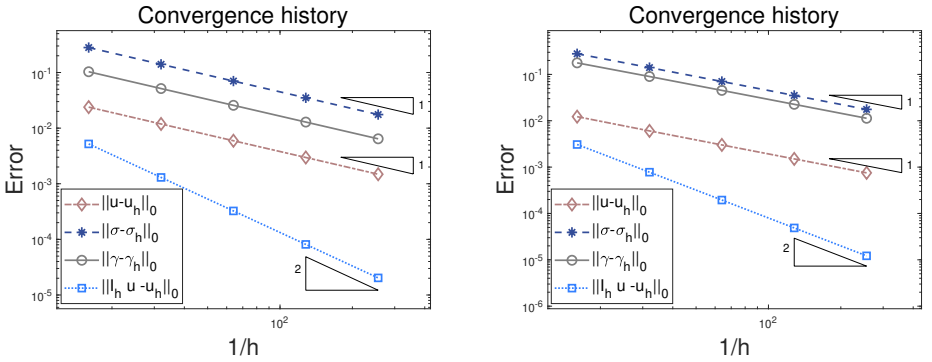

FIG. 7. *Convergence history for square grids (left) and trapezoidal grids with* $\alpha = 0.4$ *(right) for* $\lambda = 1$.

and the load f given by

$$f = \begin{pmatrix} 2\pi^2 \sin(\pi x)\sin(\pi y) \\ 2\pi^2 \cos(\pi x)\cos(\pi y) \end{pmatrix}.$$

Here, we choose $\mu = 1$ and $\lambda = \{1, 10^3, 10^4\}$. The solution (5.1) has vanishing divergence in the limit $\lambda \to +\infty$. This, together with the fact that f does not depend on λ, makes this test case suitable for checking numerically that our proposed method is indeed locking free (cf. [24]). We consider square grids and trapezoidal grids with $\alpha = 0.4$ (cf. Figure 4) to verify the convergence rates. The convergence history against the mesh size is displayed in Figures 7–9 for $\lambda = 1$, $\lambda = 10^3$, and $\lambda = 10^4$, respectively. As expected, optimal convergence rates can be obtained for all the cases, and, in addition, second order convergence can be achieved for $\|I_h u - u_h\|_0$. Moreover, all the errors seem to have similar values when different values of λ are exploited, which means our method is locking free and the errors do not depend on λ.

5.3. Singular solution on L-shaped domain. In this example, we consider the L-shaped domain $\Omega = (-1,1)\times(-1,1)\backslash(0,1)\times(0,1)$, where the exact solution is given by (cf. [30])

$$u(x,y) = (x^2+y^2)^{\beta}\begin{pmatrix} 1 \\ 1 \end{pmatrix}, \quad \beta \geq 0.$$

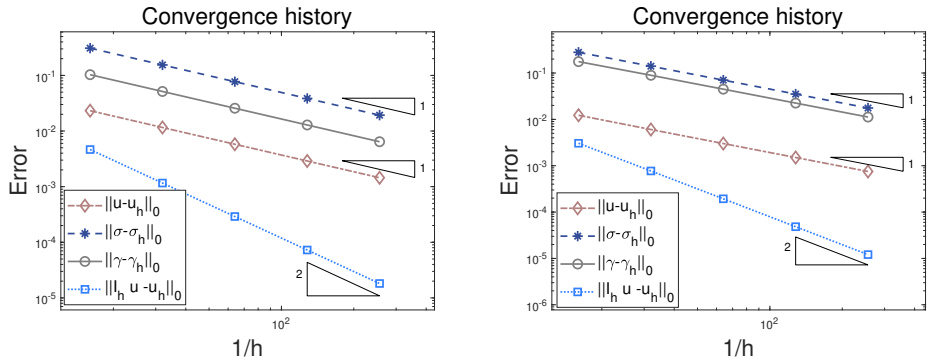

FIG. 8. *Convergence history for square grids (left) and trapezoidal grids with* $\alpha = 0.4$ *(right) for* $\lambda = 10^3$.

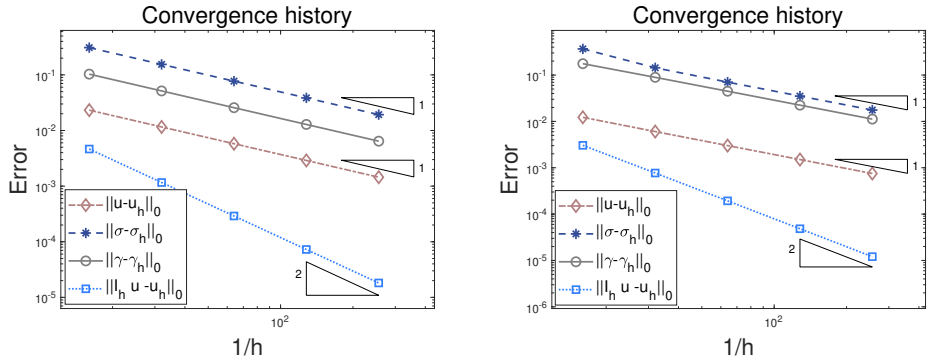

FIG. 9. *Convergence history for square grids (left) and trapezoidal grids with* $\alpha = 0.4$ *(right) for* $\lambda = 10^4$.

We first choose β as $1/3$. With this choice of β, u is in $H^r(\Omega;\mathbb{R}^2)$ for any $0 \le r < 2\beta+1$ ($\simeq 1.67$). Here, we choose the material parameters as $\mu = 1$ and $\lambda = 1$. We use uniform square grids and h-perturbation grids (cf. Figure 10) in our numerical experiment. Expected convergence rates matching the theoretical results can be observed in Figure 11.

Next, we choose β to be $1/12$, in which case u is in $H^r(\Omega;\mathbb{R}^2)$ for any $0 \le r < 2\beta+1$ ($\simeq 1.167$). Again, we show the convergence history for all the errors involved in Figure 12 by using square grids and h-perturbation grids as shown in Figure 10. We can observe from Figure 12 that the convergence rates for $\|u-u_h\|_0$ and $\|I_h u-u_h\|_0$ are approximately 0.8, which is better than the expected convergence rate 2ϵ ($\epsilon = 2\beta$). We remark that it is difficult to give an interpretation to the observed convergence rates for $\|u-u_h\|_0$ and $\|I_h u-u_h\|_0$ with the sole results of Theorem 3.4 and Remark 3.5. On the other hand, we can observe that the convergence rate for L^2 errors of $\boldsymbol{\sigma}$ and γ is about 0.167, which matches our theory given in Theorem 3.3.

5.4. Solution on L-shaped domain with low regularity. Next, we test a benchmark example, which exhibits re-entrant corner singularity at the origin $(0,0)$ (cf. [2]). Let Ω be a polygonal domain with vertices $(0,0)$, $(-1,-1)$, $(1,-1)$, $(1,1)$,

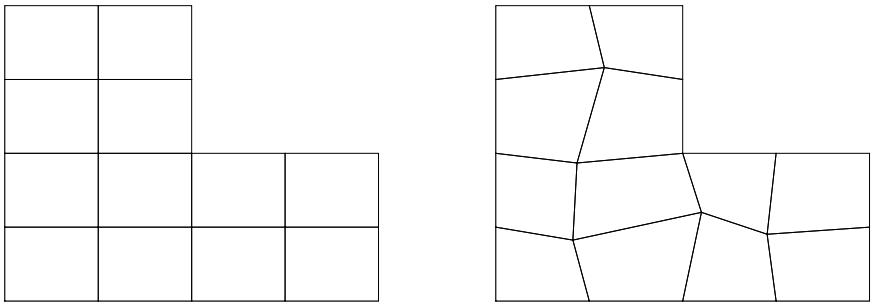

FIG. 10. *Initial grid: square grid (left) and h-perturbation grid (right).*

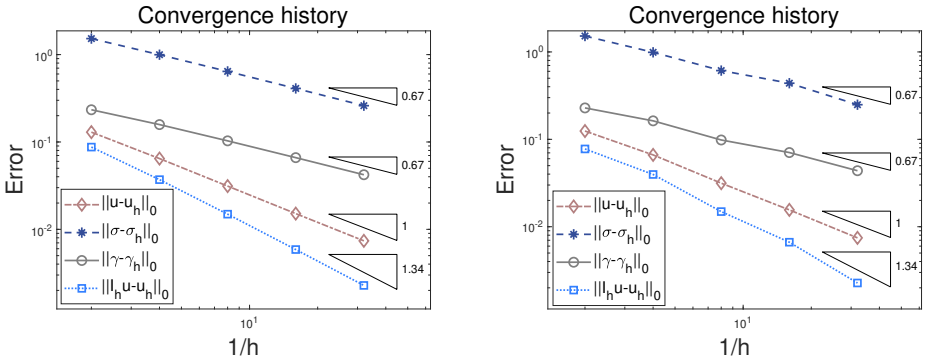

FIG. 11. *Convergence history for square grid (left) and h-perturbation grid (right) for the example in section* 5.3 *with* $\beta = 1/3$.

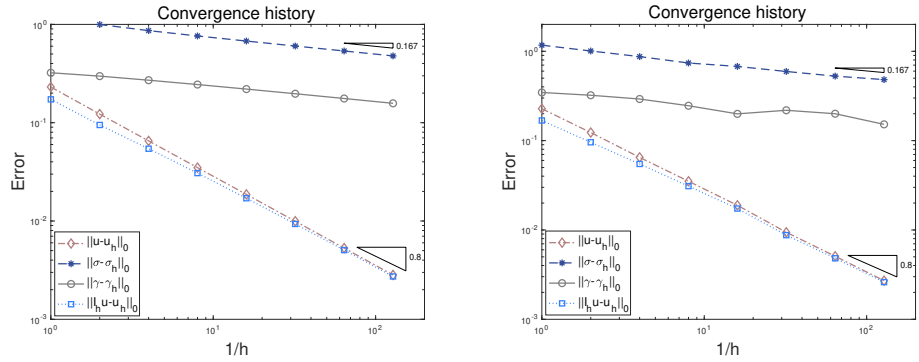

FIG. 12. *Convergence history for square grid (left) and h-perturbation grid (right) for the example in section* 5.3 *with* $\beta = 1/12$.

$(-1, 1)$, and $f = 0$. The exact solution is given by its polar coordinates

$$u(r,\theta) = \begin{pmatrix} u_r(r,\theta)\cos(\theta) - u_\theta(r,\theta)\sin(\theta) \\ u_r(r,\theta)\sin(\theta) + u_\theta(r,\theta)\cos(\theta) \end{pmatrix},$$

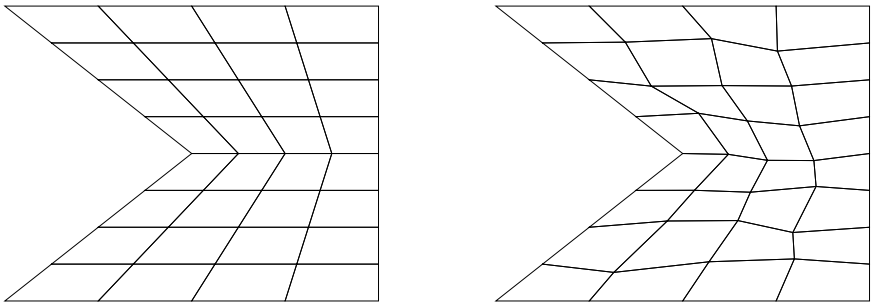

FIG. 13. *Schematic of the grids employed for the example in section* 5.4.

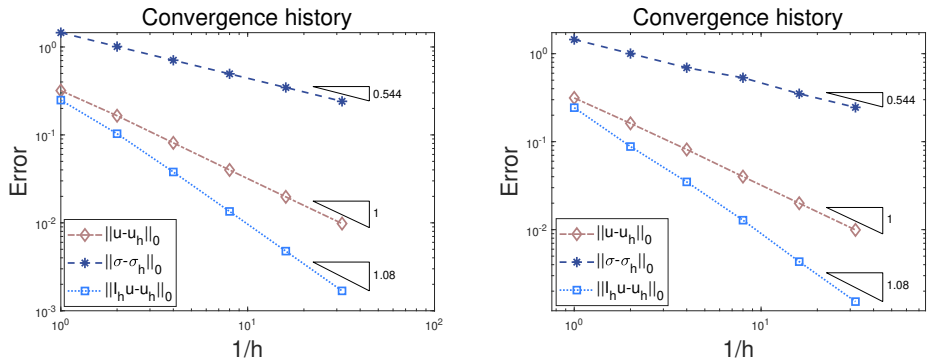

FIG. 14. *Convergence history for square grids (left) and h-perturbation grids (right) for the example in section* 5.4.

where $u_r(r,\theta)$ and $u_\theta(r,\theta)$ are given by

$$u_r(r,\theta) = \frac{1}{2\mu} r^\delta \Big(-(\delta+1)\cos((\delta+1)\theta) + (C_2 - (\delta+1))C_1 \cos((\delta-1)\theta)\Big),$$
$$u_\theta(r,\theta) = \frac{1}{2\mu} r^\delta \Big((\delta+1)\sin((\delta+1)\theta) + (C_2 + \delta - 1)C_1 \sin((\delta-1)\theta)\Big),$$

and

$$C_1 = -\frac{\cos((\delta+1)\omega)}{\cos((\delta-1)\omega)}, \quad C_2 = \frac{2(\lambda+2\mu)}{\lambda+\mu}.$$

Here $\delta \approx 0.544484$ is the critical exponent which can be obtained by solving

$$\delta \sin(2\omega) + \sin(2\omega\delta) = 0$$

with $\omega = \frac{3\pi}{4}$.

We employ the square grids and h-perturbation of square grids as shown in Figure 13. The convergence history against the mesh size for both grids is displayed in Figure 14. We can observe that the convergence rates match our proposed theories; in addition, $\|I_h u - u_h\|_0$ has slightly better convergence rate than $\|u - u_h\|_0$.

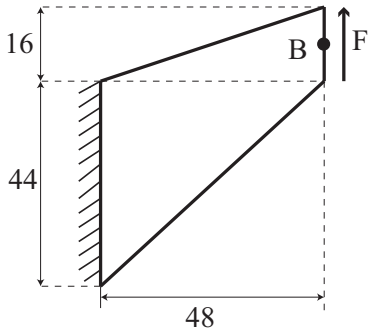

FIG. 15. *Configuration for Cook's membrane test case.*

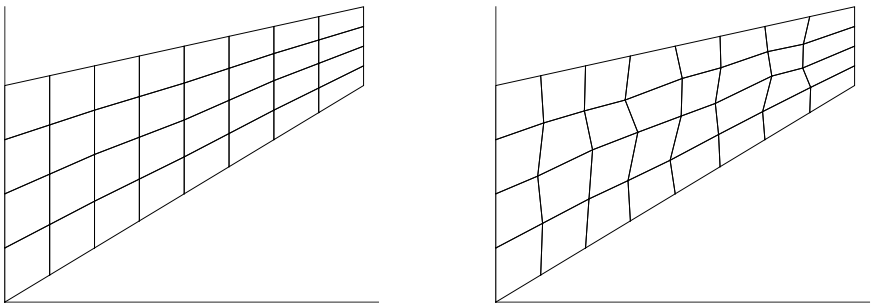

FIG. 16. *Initial grid: quadrilateral grid (left) and h-perturbation grid (right).*

5.5. Cook's membrane test case. We next consider a bending dominated test case widely used in the mechanical engineering literature and referred to as Cook's membrane; see Figure 15 for a description of the domain and of the boundary conditions. Following [9], we take a quasi-incompressible material with $\mu = 0.375$ and $\lambda = 7.5 \times 10^6$. The load F is uniform and has unitary resultant. Convergence results are reported in terms of the number of degrees of freedom monitoring u_B; the horizontal and vertical displacements at point B ($x_B = (48, 52)$) are denoted by $u_{h,1}(x_B)$ and $u_{h,2}(x_B)$, which can be approximated as the mean values of all triangles belonging to $\mathcal{T}_h$ which share the common node B. Quadrilateral grids and h-perturbation grids are employed in the simulation (cf. Figure 16). The displacement at point B with quadrilateral grid is reported in Figure 17, which is quite close to the reference value given in [24]. In addition, the results displayed in Figure 18 indicate that similar results can be observed by using h-perturbation grids.

6. Conclusion. In this paper, we have developed a lowest order SDG method for linear elasticity on general polygonal meshes. This new approach earns low degrees of freedom and is computationally efficient. In addition, hanging nodes are allowed, which can be simply treated as additional vertices. A priori error estimates for stress, displacement, and rotation covering low regularities are given. Some benchmark examples are chosen to verify the proposed theories. The numerical results indicate that the proposed method is locking free and allows rough grids. Our future work includes the design of adaptive mesh refinement strategies based on suitable a posteriori error estimators.

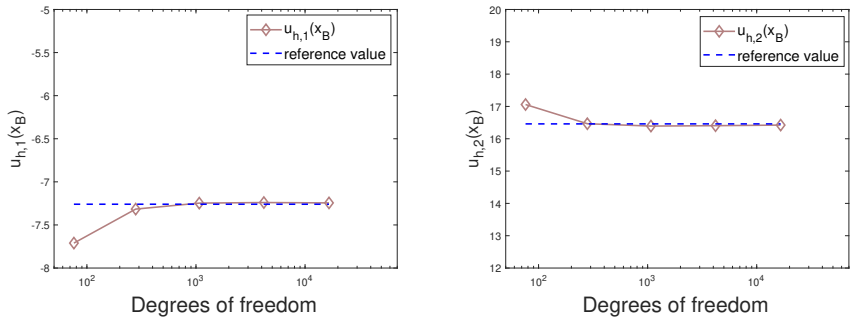

FIG. 17. *Convergence of the displacement at B with quadrilateral grid: $u_{h,1}(x_B)$ and $u_{h,2}(x_B)$.*

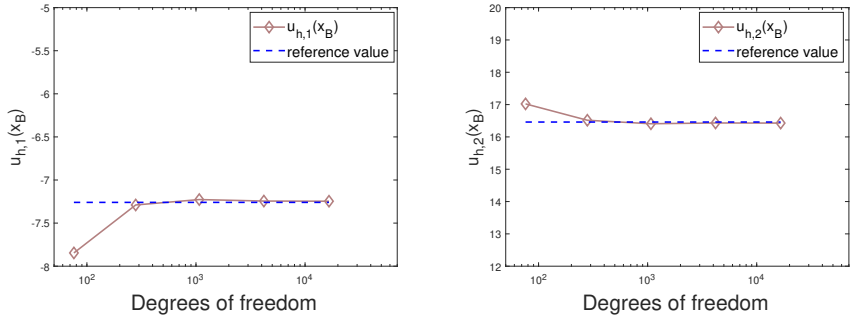

FIG. 18. *Convergence of the displacement at B with h-perturbation grid: $u_{h,1}(x_B)$ and $u_{h,2}(x_B)$.*

Acknowledgment. The authors would like to express their sincere thanks to the anonymous referees, whose invaluable comments led to an improved version of the paper.

REFERENCES

[1] S. ADAMS AND B. COCKBURN, *A mixed finite element method for elasticity in three dimensions*, J. Sci. Comput., 25 (2005), pp. 515–521, https://doi.org/10.1007/s10915-004-4807-3.

[2] J. ALBERTY, C. CARSTENSEN, S. A. FUNKEN, AND R. KLOSE, *Matlab implementation of the finite element method in elasticity*, Computing, 69 (2002), pp. 239–263, https://doi.org/10.1007/s00607-002-1459-8.

[3] T. ARBOGAST, M. F. WHEELER, AND I. YOTOV, *Mixed finite elements for elliptic problems with tensor coefficients as cell-centered finite differences*, SIAM J. Numer. Anal., 34 (1997), pp. 828–852, https://doi.org/10.1137/S0036142994262585.

[4] D. N. ARNOLD, D. BOFFI, AND R. S. FALK, *Quadrilateral $H(div)$ finite elements*, SIAM J. Numer. Anal., 42 (2005), pp. 2429–2451, https://doi.org/10.1137/S0036142903431924.

[5] D. N. ARNOLD, F. BREZZI, AND J. DOUGLAS, *PEERS: A new mixed finite element for plane elasticity*, Japan J. Appl. Math., 1 (1984), pp. 347–367, https://doi.org/10.1007/BF03167064.

[6] D. N. ARNOLD, J. DOUGLAS, AND C. P. GUPTA, *A family of higher order mixed finite element methods for plane elasticity*, Numer. Math., 45 (1984), pp. 1–22, https://doi.org/10.1007/BF01379659.

[7] D. N. ARNOLD, R. S. FALK, AND R. WINTHER, *Differential complexes and stability of finite element methods.* II: *The elasticity complex*, in Compatible Spatial Discretizations, D. Arnold, P. Bochev, R. Lehoucq, R. Nicolaides, and M. Shashkov, eds., IMA Vol. Math. Appl. 142, Springer-Verlag, New York, 2005, pp. 47–67.

[8] E. Artioli, S. de Miranda, C. Lovadina, and L. Patruno, *A stress/displacement virtual element method for plane elasticity problems*, Comput. Methods Appl. Mech. Engrg., 325 (2017), pp. 155–174, https://doi.org/10.1016/j.cma.2017.06.036.

[9] F. Auricchio, L. Beirão Da Veiga, C. Lovadina, and A. Reali, *An analysis of some mixed-enhanced finite element for plane linear elasticity*, Comput. Methods Appl. Mech. Engrg., 194 (2005), pp. 2947–2968, https://doi.org/10.1016/j.cma.2004.07.028.

[10] I. Babuška and A. K. Aziz, *Survey lectures on the mathematical foundations of the finite element method*, in The Mathematical Foundations of the Finite Element Method with Applications to Partial Differential Equations, A. K. Aziz, ed., Academic Press, New York, 1972, pp. 1–359.

[11] I. Babuška and M. Suri, *Locking effects in the finite element approximation of elasticity problems*, Numer. Math., 62 (1992), pp. 439–463, https://doi.org/10.1007/BF01396238.

[12] I. Babuška and B. Szabo, *On the rates of convergence of the finite element method*, Internat. J. Numer. Methods Engrg., 18 (1982), pp. 323–341, https://doi.org/10.1002/nme.1620180302.

[13] L. Beirão Da Veiga, F. Brezzi, A. Cangiani, G. Manzini, L. D. Marini, and A. Russo, *Basic principles of virtual element methods*, Math. Models Methods Appl. Sci., 23 (2013), pp. 199–214, https://doi.org/10.1142/S0218202512500492.

[14] L. Beirão Da Veiga, F. Brezzi, and L. D. Marini, *Virtual elements for linear elasticity problems*, SIAM J. Numer. Anal., 51 (2013), pp. 794–812, https://doi.org/10.1137/120874746.

[15] D. Boffi, F. Brezzi, and M. Fortin, *Reduced symmetry elements in linear elasticity*, Commun. Pure Appl., 8 (2009), pp. 95–121, https://doi.org/10.3934/cpaa.2009.8.95.

[16] S. C. Brenner and L. R. Scott, *The Mathematical Theory of Finite Element Methods*, Springer-Verlag, New York, 2008.

[17] A. Cangiani, E. H. Georgoulis, T. Pryer, and O. J. Sutton, *A posteriori error estimates for the virtual element method*, Numer. Math., 137 (2017), pp. 857–893, https://doi.org/10.1007/s00211-017-0891-9.

[18] E. T. Chung and B. Engquist, *Optimal discontinuous Galerkin methods for wave propagation*, SIAM J. Numer. Anal., 44 (2006), pp. 2131–2158, https://doi.org/10.1137/050641193.

[19] E. T. Chung and B. Engquist, *Optimal discontinuous Galerkin methods for the acoustic wave equation in higher dimensions*, SIAM J. Numer. Anal., 47 (2009), pp. 3820–3848, https://doi.org/10.1137/080729062.

[20] E. T. Chung, E.-J. Park, and L. Zhao, *Guaranteed a posteriori error estimates for a staggered discontinuous Galerkin method*, J. Sci. Comput., 75 (2018), pp. 1079–1101, https://doi.org/10.1007/s10915-017-0575-8.

[21] P. G. Ciarlet, *The Finite Element Method for Elliptic Problems*, North-Holland, Amsterdam, 1978.

[22] B. Cockburn and K. Shi, *Superconvergent HDG methods for linear elasticity with weakly symmetric stresses*, IMA J. Numer. Anal., 33 (2013), pp. 747–770, https://doi.org/10.1093/imanum/drs020.

[23] B. F. de Veubeke, *Stress function approach*, in Proceedings of the World Congress on Finite Element Methods in Structural Mechanics, Bournemouth, 1975, pp. J.1–J.51.

[24] D. A. Di Pietro and A. Ern, *A hybrid high-order locking-free method for linear elasticity on general meshes*, Comput. Methods Appl. Mech. Engrg., 283 (2015), pp. 1–21, https://doi.org/10.1016/j.cma.2014.09.009.

[25] J. Djoko, B. Lamichhane, B. Reddy, and B. Wohlmuth, *Conditions for equivalence between the Hu–Washizu and related formulations, and computational behavior in the incompressible limit*, Comput. Methods Appl. Mech. Engrg., 195 (2006), pp. 4161–4178, https://doi.org/10.1016/j.cma.2005.07.018.

[26] A. Ern and J.-L. Guermond, *Quasi-optimal nonconforming approximation of elliptic PDEs with contrasted coefficients and minimal regularity*, 2018, https://hal.archives-ouvertes.fr/hal-01964299.

[27] R. S. Falk, *Nonconforming finite element methods for the equations of linear elasticity*, Math. Comp., 57 (1991), pp. 529–550, https://doi.org/10.1090/S0025-5718-1991-1094947-6.

[28] P. Grisvard, *Elliptic Problems in Nonsmooth Domains*, Pitman, Boston, 1985.

[29] B. P. Lamichhane, *Inf–sup stable finite-element pairs based on dual meshes and bases for nearly incompressible elasticity*, IMA J. Numer. Anal., 29 (2009), pp. 404–420, https://doi.org/10.1093/imanum/drn013.

[30] J. J. Lee and H. H. Kim, *Analysis of a staggered discontinuous Galerkin method for linear elasticity*, J. Sci. Comput., 66 (2016), pp. 625–649, https://doi.org/10.1007/s10915-015-0036-1.

[31] T. P. Mathew, *Domain Decomposition and Iterative Refinement Methods for Mixed Finite Element Discretizations of Elliptic Problems*, Ph.D. thesis, Tech. report 463, Courant Institute of Mathematical Sciences, New York University, New York, 1989.

[32] T. H. Ong, T. T. Phuong Hoang, S. P. Bordas, and H. Nguyen-Xuan, *A staggered cell-centered finite element method for compressible and nearly-incompressible linear elasticity on general meshes*, SIAM J. Numer. Anal., 53 (2015), pp. 2051–2073, https://doi.org/10.1137/140990103.

[33] S.-C. Soon, B. Cockburn, and H. K. Stolarski, *A hybridizable discontinuous Galerkin method for linear elasticity*, Internat. J. Numer. Methods Engrg., 80 (2009), pp. 1058–1092, https://doi.org/10.1002/nme.2646.

[34] R. Stenberg, *A family of mixed finite elements for the elasticity problem*, Numer. Math., 53 (1988), pp. 513–538, https://doi.org/10.1007/BF01397550.

[35] M. Vogelius, *An analysis of the p-version of the finite element method for nearly incompressible materials*, Numer. Math., 41 (1983), pp. 39–53, https://doi.org/10.1007/BF01396304.

[36] C. Wang, J. Wang, R. Wang, and R. Zhang, *A locking-free weak Galerkin finite element method for elasticity problems in the primal formulation*, J. Comput. Appl. Math., 307 (2016), pp. 346–366, https://doi.org/10.1016/j.cam.2015.12.015.

[37] L. Zhao and E.-J. Park, *Fully computable bounds for a staggered discontinuous Galerkin method for the Stokes equations*, Comput. Math. Appl., 75 (2018), pp. 4115–4134, https://doi.org/10.1016/j.camwa.2018.03.018.

[38] L. Zhao and E.-J. Park, *A staggered discontinuous Galerkin method of minimal dimension on quadrilateral and polygonal meshes*, SIAM J. Sci. Comput., 40 (2018), pp. A2543–A2567, https://doi.org/10.1137/17M1159385.

[39] L. Zhao and E.-J. Park, *A lowest-order staggered DG method for the coupled Stokes–Darcy problem*, IMA J. Numer. Anal., (2020), drz048, https://doi.org/10.1093/imanum/drz048.

[40] L. Zhao, E.-J. Park, and D.-w. Shin, *A staggered DG method of minimal dimension for the Stokes equations on general meshes*, Comput. Methods Appl. Mech. Engrg., 345 (2019), pp. 854–875, https://doi.org/10.1016/j.cma.2018.11.016.